

Sculpting Asymmetric, Hollow-Core, Three-Dimensional Nanostructures Using Colloidal Particles

Xu A. Zhang, Bin Dai, Zhiyuan Xu, and Chih-Hao Chang*

Colloidal elements have historically played a key role in “bottom-up” self-assembly processes for nanofabrication. However, these elementary components can also interact with light to generate complex intensity distributions and facilitate “top-down” lithography. Here, a nanolithography technique is demonstrated based on oblique illuminations of colloidal particles to fabricate hollow-core 3D nanostructures with complex symmetry. The light–particle interaction generates an angular light distribution as governed by Mie scattering, which can be compounded by multiple illuminations to sculpt novel 3D structures in the underlying photoresist. The fabricated geometry can be controlled by the particle parameters and illumination configurations, enabling the fabrication of a large variety of asymmetric hollow nanostructures. The proposed technique has high pattern versatility, is low cost and high throughput, and can find potential application in nanoneedles, nanonozzles, and materials with anisotropic properties.

1. Introduction

Three-dimensional (3D) nanostructures have received significant research interests, and exhibit many unique properties such as photonic/phononic bandgaps,^[1–4] enhanced energy conversions,^[5,6] antireflection,^[7,8] and self-cleaning.^[7,8] One interesting subgroup of 3D nanostructures are hollow-core structures, where hollow nanoparticles and microneedles have been studied for drug delivery applications,^[9–14] spherical nanoshells can be used for broadband light trapping in solar cells,^[15] and hollow metal structures have extensive applications in plasmonics and photonics.^[16,17] Another interesting subgroup are tilted structures lacking mirror symmetry along one axis, which can induce anisotropic material properties.^[18–34] The well-known directional adhesion of gecko's foot is enabled by the tilted arrangements of setae and spatula.^[19] The hierarchical groove-like structures on butterfly wings exhibit anisotropic wetting, where water droplets

on the wing can only roll off away from the insect's body while being pinned in the opposite direction.^[20]

These bio-inspired principles have led to considerable research on fabrication techniques to engineer artificial biomimetic nanostructures. Gecko foot-like structures have been realized using directional reactive-ion etching (RIE) and soft lithography,^[21,22] directed growth of carbon nanotubes,^[23] and electron/ion beam bombardments.^[24,25] Engineered slanted surface structures with anisotropic wetting properties have been achieved using oblique-angle microlithography,^[26,31–33] mechanical deformation,^[27] and holographic lithography,^[28] and structures with more complex symmetry can be achieved by using multiple exposures and elastocapillary self-assembly.^[29,30,34] While these existing techniques can enable slanted microstructures, controlling geometry other than tilt angle can be difficult. In addition, these techniques are all limited to solid structures, and tilted hollow-core structures have not been realized.

In another approach, colloidal particles have shown promise as a facile nanofabrication technique, where they can be used as elementary elements for self-assembly systems.^[35–38,46] Colloidal elements can also be integrated in planar micromachining processes, where they are used as physical masks for additive,^[39–41,46] subtractive,^[42,46] and replication processes.^[43–45] Colloidal particles can also be used for optical lithography to pattern 2D nanostructures without

X. A. Zhang, B. Dai, Z. Xu, Prof. C.-H. Chang
Department of Mechanical and Aerospace Engineering
North Carolina State University
Raleigh, North Carolina 27695, USA
E-mail: chichang@ncsu.edu



DOI: 10.1002/sml.201402750

any external hardware.^[47–51] Beyond 2D patterning, we have recently demonstrated that close-packed colloidal arrays can also be used to fabricate periodic 3D nanostructures with tunable lattice parameters,^[52] and particle light scattering can be employed to fabricate hollow-core “nano-volcanoes.”^[53] By harnessing the optical interaction with colloidal elements, complex 3D structure can be patterned at extremely low cost.

In this work, we demonstrate a 3D nanolithography technique using multiple oblique illuminations of colloidal particles to make hollow-core asymmetric nanostructures. The particle-light interaction results in complex intensity patterns, which can be used to expose underlying photosensitive materials. Multiple sequential exposures in various configurations can be used to sculpt the final structure and enable more complex symmetry. The proposed method allows the design of 3D structure with additional fabrication parameters, such as incident angle, polarization, dose, and exposure configurations. The light scattering is chosen in Mie scattering regime ($D \sim \lambda$), where the scattering pattern has alternating bright and dark lobe-like angular distribution with high intensity contrast. In this regime the pattern is highly sensitive to the particle size to wavelength ratio, enabling high diversity of fabricated nanostructures. The proposed process relies solely on particle-light interactions, and does not require complex hardware often seen in existing 3D nanolithography systems such as electron-beam/focused-ion beam,^[54] interference/holographic,^[55] and multi-photon lithography.^[56–58] Since the scattering mechanisms do not rely on coherence, lasers are not required and any narrowband light source can be used. Harnessing the particle-light interactions also enable novel local scattering patterns, and expands on the use of colloidal elements beyond self-assembly systems. The particles are assembled directly on the photoresist surface, ensuring intimate contact between the colloidal particles and the photoresist. Isolated colloidal particles are the focus of this work, but the proposed method can also be applied to multiple particles, non-spherical colloids and their assemblies to fabricate exotic nanostructures.^[59,60] Plasmonic interaction using metal particles to fabricate subwavelength surface features is also of interest, and it is currently under investigation.

The proposed fabrication method of slanted nanostructures is shown in **Figure 1**, where light scattering intensity pattern generated by oblique illumination of a single nanoparticle is recorded by underlying photosensitive resist. Using a positive resist, consecutive exposures can be used to remove material and sculpt the final geometry. The oblique exposure is at angle θ , as shown in Figure 1(b), and can be controlled to yield various scattering patterns. A cross section of the 3D intensity pattern from the finite difference time domain (FDTD) simulation using transverse-magnetic (TM) polarized illumination at $\theta = 40^\circ$, $\lambda = 325$ nm, and $D = 390$ nm is shown in Figure 1(a).^[61] In this configuration the electric field is aligned along the plane of incidence under TM polarized illumination, while being orthogonal to the plane of incidence under transverse-electric (TE) polarized illumination. The intensity pattern in the resist shows distinct lobe-like angular variations with a highly focused central lobe and multiple side lobes. The lobes closest to the central lobe are defined as first side lobes, the second closest as second side lobes, and so

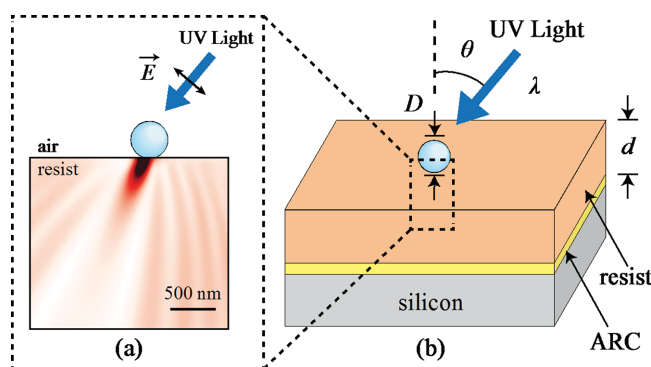


Figure 1. Fabrication process of hollow asymmetric 3D nanostructures using oblique light illumination of a colloidal nanoparticle. (a) FDTD simulation illustrating a cross-section of the scattering intensity pattern produced by TM-polarized UV light at 40° and a single polystyrene nanoparticle. Red and white contours indicate high and low intensities, respectively. (b) The intensity pattern is recorded by an underlying photoresist layer on top of an ARC layer. Multiple oblique illuminations can be used to pattern complex structure symmetry.

on. Compared with the normal illumination case,^[53] the scattering system loses symmetry within the plane of incidence, and the magnitude and distribution of the oblique scattering intensity pattern are largely altered. As a result, the oblique scattering pattern cannot be regarded as a pure rotation of the normal scattering pattern. The repeatability of the proposed technique can be ensured by controlling lithography parameters such as wavelength, particle diameters, illumination configuration, and exposure dose, which can be precisely controlled.

2. Results and Discussion

The fabricated slanted hollow 3D nanostructures are shown in the scanning electron microscope (SEM) images depicted in **Figure 2**. The exposures were conducted using a 325 nm wavelength laser and 390 nm diameter polystyrene nanoparticles. The first row illustrates the side views of the fabricated structures under TM-polarized illumination with incident angles $\theta = 20^\circ, 30^\circ, 45^\circ$, and 70° . The corresponding cross-sectional views are displayed in the second row, indicating the hollow cores of the structures. The third row illustrates the side views of the nanostructures fabricated under TE-polarized illumination with incident angles $\theta = 30^\circ, 45^\circ, 60^\circ$, and 70° . The inset in each image is the simulated nanostructure using FDTD simulation and binary resist model (for details see Supplementary Information A). In the TM case, highly focused central lobe generates slanted nanostructures with hollow chambers, which are enclosed by complete shells formed by the first side lobes. Shells formed by the second or higher order side lobes are usually broken due to mechanical instability, as observed in the $\theta = 20^\circ$ and 30° cases. When $\theta = 45^\circ$, the second shell is preserved, forming a double-shell slanted nanostructure, while when $\theta = 70^\circ$, the first and second side lobes on the left merge to form a thick wall, and the second shell collapsed on the right. The structures from high incident angles ($\theta \geq 45^\circ$) are more slanted than those from low incident angles owing to the effects of

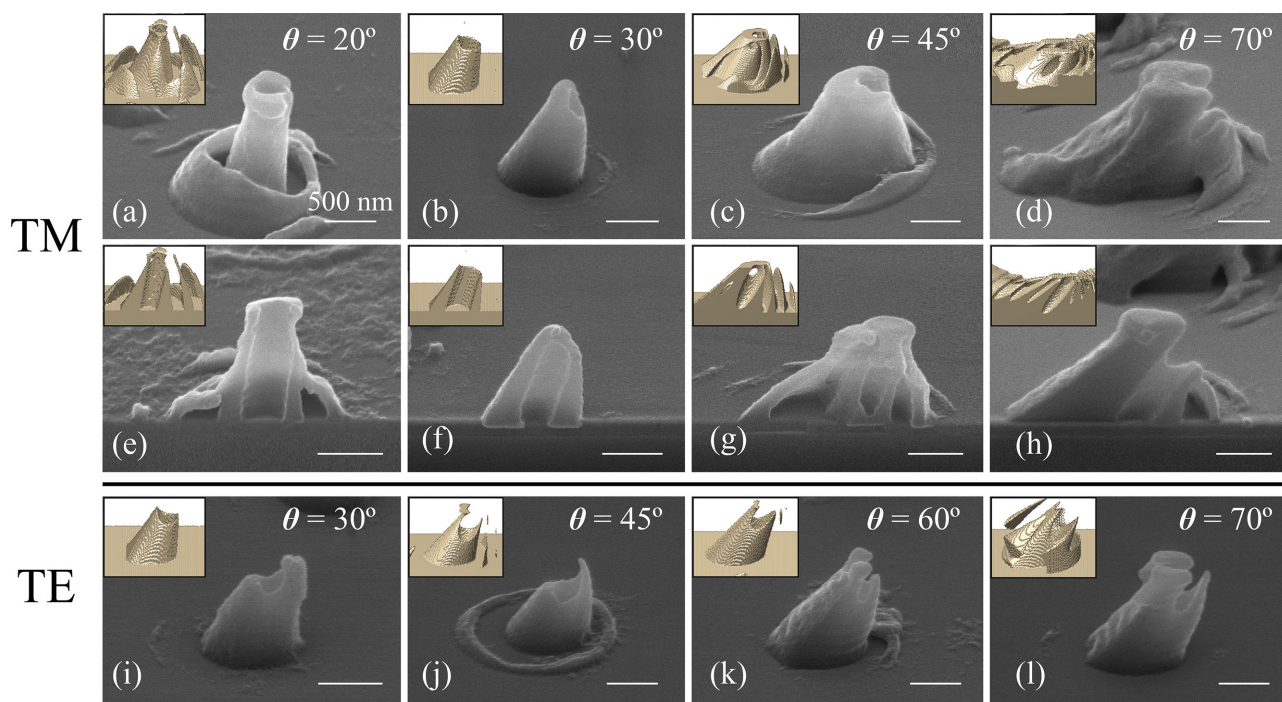


Figure 2. Micrographs of the fabricated asymmetric slanted hollow 3D nanostructures using TE and TM-polarized 325 nm illuminations and a 390 nm diameter nanosphere. (a)–(d) Incident angle $\theta = 20^\circ, 30^\circ, 45^\circ,$ and 70° and exposure doses of $110 \text{ mJ cm}^{-2}, 135 \text{ mJ cm}^{-2}, 110 \text{ mJ cm}^{-2},$ and $290 \text{ mJ cm}^{-2},$ respectively, under TM polarized illumination. (e)–(h) Corresponding cross-sections of (a)–(d). (i)–(l) Incident angle $\theta = 30^\circ, 45^\circ, 60^\circ,$ and 70° and exposure doses of $150 \text{ mJ cm}^{-2}, 163 \text{ mJ cm}^{-2}, 268 \text{ mJ cm}^{-2},$ and $435 \text{ mJ cm}^{-2},$ respectively, under TE polarized illumination. The inset diagrams show the corresponding simulated nanostructures using FDTD method and a binary resist model.

second side lobes. The exposure dose can greatly affect structure dimensions in oblique illumination, and the strategy for determining proper exposure dosage can be found in Supplementary Information B.

The structure from TM polarization and $\theta = 30^\circ$ is of particular interest. It consists of a sharp tip with radius of curvature of $\sim 90 \text{ nm}$, a hollow chamber with small volume, and an opening on the side, resembling a nanoscale needle. This type of structure may find applications in transdermal and intercellular drug delivery with precise dose control. The nanostructures typically have less geometry variety in TE cases as opposed to TM, because the electric field is orthogonal to the plane of incident and does not change direction for different incident angles. There is a single sharp feature on the incidence side while the features are broken on the opposite side, as in Figure 2(i) and (j) or preserved, as in Figure 2(k) and (l).

The sidewall and center hole angles with respect to incident angle are analyzed for the slanted nanostructures fabricated from TM-polarized cases, as shown in Figure 3 (see Figure S3 in Supplementary Information C for images of additional fabricated structures used in this analysis). The center hole angle β_c is defined as the angle between the normal axis of the hole and the horizontal plane, and the sidewall angles β_L and β_R are the inner angles of the left and right sidewalls, respectively. Subscripts “1” and “2” denote the sidewalls determined by the first and second side lobes, respectively. If $\beta_L < \beta_R$, as the case depicted in the schematic, the structure is slanted towards right, and vice versa if $\beta_L > \beta_R$. The analysis is based on incidence from the right, resulting

in the structure slanted towards right and $\beta_L < \beta_R$ for both first and second shells. Starting from equal sidewall angles at normal incidence, the left sidewall angle decreases while the right one increases with increasing incident angle, indicating more slanted left sidewalls. The first shell always exists for the entire 70° incidence range while the second shell appears after 45° due to the angular function of the scattering pattern.

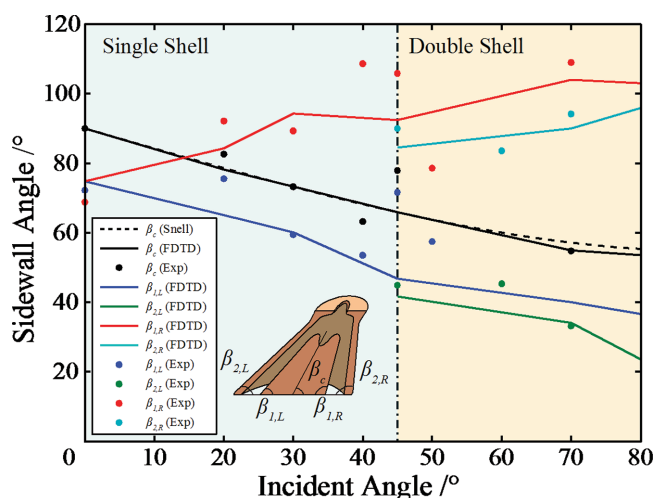


Figure 3. Sidewall angle and center hole angle analysis of the slanted nanostructure with respect to illumination incident angle. The samples are fabricated using TM-polarized 325 nm illumination and a 390 nm diameter nanosphere. The angles are defined in the schematic between the outer surface and the horizontal plane. The experimental data agrees well with theoretical models using FDTD and Snell’s law.

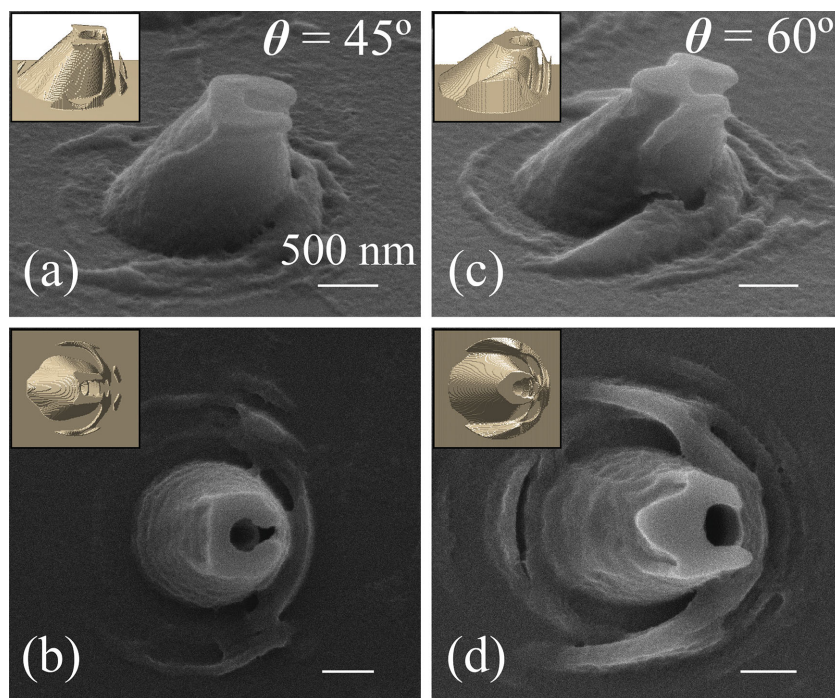


Figure 4. Micrographs of the fabricated asymmetric hollow 3D nanostructures using TM-polarized 325 nm illuminations and a 500 nm diameter nanosphere. The (a) side and (b) top views of the nanostructure fabricated at incident angle $\theta = 45^\circ$ and exposure dose of 150 mJ cm^{-2} . The (c) side and (d) top views of the nanostructure fabricated at incident angle $\theta = 60^\circ$ and exposure dose of 200 mJ cm^{-2} . The inset diagrams show the corresponding simulated nanostructures using FDTD method and a binary resist model.

The second shell angles are lower than the first shell angles on the same side, meaning increased obliqueness of the outermost surface of the nanostructure. This behavior is unique because of the existence of higher order side lobes in the scattering intensity pattern, compared to the oblique microlithography which adopts the non-diffractive shadowing effect.^[31–33] The center hole angle closely follows Snell's law when ignoring the nanosphere for both FDTD simulation and experiments, indicating the particle has negligible effect on the center hole angle.

Various types of nanostructures can be achieved by using different sphere sizes, since scattering effect is sensitive to the particle diameter in the Mie regime. Two examples are depicted in **Figure 4** with 500 nm diameter nanospheres at 45° and 60° TM incidence. The structures are hollow, but the surface morphologies are different from the ones in **Figure 2** due to different scattering intensity patterns. Additional single exposure results using 760 nm and 1 μm diameter spheres can be found in **Figure S4** of Supplementary Information C. Other geometries can be achieved by varying exposure wavelength, particle geometry such as non-spherical colloids, and particle material such as metal and silica particles.

The use of multiple illuminations is also explored to create 3D structures with more complex symmetry. Analogous to a sculpting knife carving away materials, the exposure intensity profiles are compounded to shape the final structure. The first experiments are based on coplanar double exposures, where the first and second illuminations are arranged in the same

plane of incidence with mirror symmetry, as depicted in **Figure 5(a)**. **Figure 5(b)** and **(c)** illustrates the top- and side-view micrographs of the fabricated structures using TM polarization at 30° and 50° incidence, respectively. The results from TE polarization using the same exposure conditions are shown in **Figure 5(d)** and **(e)**. Each set of result shows a twin slanted hollow nanostructures with mirror symmetry, a direct result of the lithography conditions. The structural heights are shorter than the original photoresist thickness because the energy summation of the two scattering intensity pattern resulted in lower exposure contrast in the overlapped region. As observed in **Figure 5(b)** and **(c)**, the first shell exists for both cases while the second shell only appears in 50° incidence case, agreeing with the analysis in **Figure 3**. Sharper features are created using TE polarization, as shown in **Figure 5(d)** and **(e)**. The sculpting effect is evident in **Figure 5(d)**, where the second exposure carves the initial hollow structure into five symmetric nanoneedles with radii of curvature in the range of 30–40 nm. In this case the two scattering intensity minima are aligned to define the sharp tips. This is in contrast to the 50° case in **Figure 5(c)**,

where the intensity profiles overlap to a lesser degree and the resulting structures closely resemble the single exposure case.

The double exposure can be further generalized by adjusting the in-plane azimuth angle ϕ , as shown in **Figure 6(a)**. In this configuration, the two exposures have the same incident angle but are in different incident planes. **Figure 6(b)–(e)** show the fabricated nanostructures with varying incident and azimuth angles for different polarizations and sphere sizes. Once azimuth angle is not 180° , a small incident angle change can result in significant structural change. In **Figure 6(b)**, sharp nanoneedles are again fabricated with one central needle missing using TM polarization compared to the one using TE polarization in **Figure 5(d)**. In **Figure 6(c)**, the structure is different from the one in **Figure 6(b)**, showing a connected twin slanted hollow nanostructure despite the small incident angle difference of 15° . Connected twin structures are also seen in the TE case with incident angle of 45° and azimuth angle of 90° in **Figure 6(e)** with joint sharp tips. Separate tips are also possible by slightly increasing the exposure dose (see **Figure S5(e)** in Supplementary Information C). The simultaneous changes of sphere size and azimuth angle also alter the structure dramatically when one compares the results using 500 nm diameter spheres and $\phi = 120^\circ$, as shown in **Figure 6(d)**, with the ones using 390 nm diameter spheres and $\phi = 135^\circ$, as shown in **Figure 6(c)**. No connection structures are present in the former case, but instead there is a separate hook-like structure in the middle. Additional fabrication results using double illuminations can be found in **Figure S5** of Supplementary Information C.

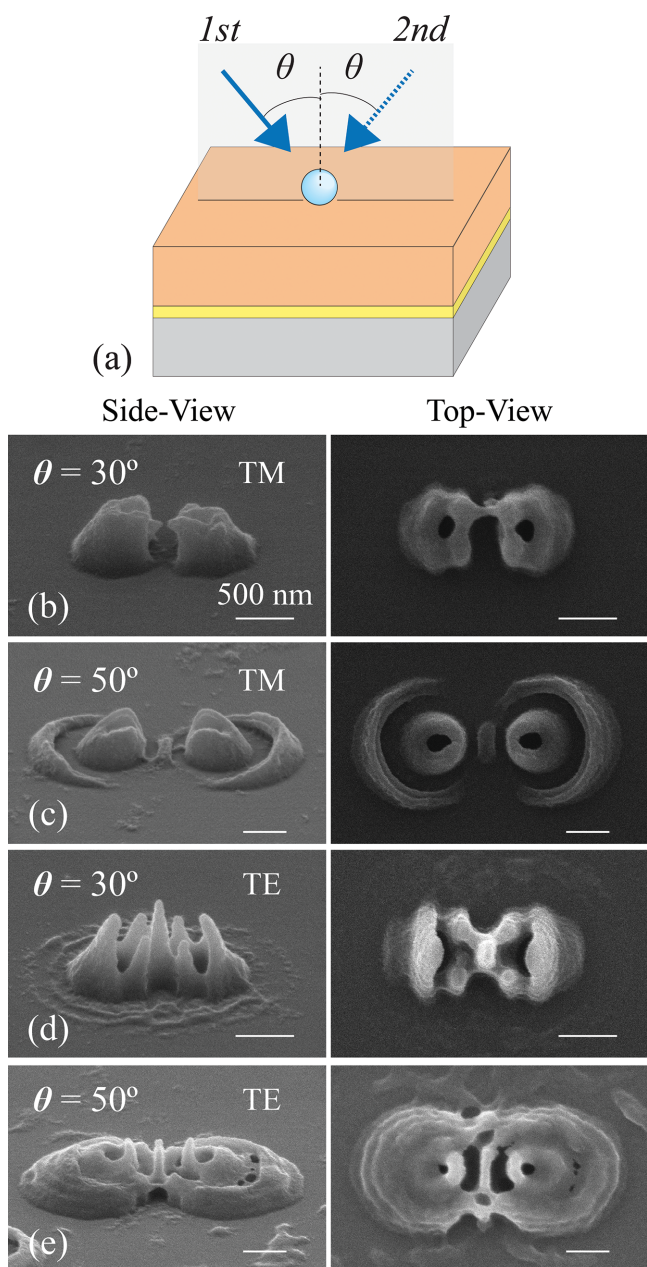


Figure 5. Micrographs of the nanostructures from sequential coplanar double exposures using 325 nm linearly polarized illuminations and a 390 nm diameter nanosphere. (a) Schematic of the exposure configuration. Side and top views of the nanostructures fabricated at (b) $\theta = 30^\circ$, exposure dose of 135 mJ cm^{-2} under TM exposures; (c) $\theta = 50^\circ$, exposure dose of 150 mJ cm^{-2} under TM exposures; (d) $\theta = 30^\circ$, exposure dose of 130 mJ cm^{-2} under TE exposures; (e) $\theta = 50^\circ$, exposure dose of 165 mJ cm^{-2} under TE exposures.

Triple and quadruple illuminations were also conducted, as shown in **Figure 7**. In these experiments, the three or four sequential exposures are arranged symmetrically with constant angle offset in reference to the sphere. The structures from triple exposures result in three-fold symmetry, and do not show significant differences between TM and TE polarizations, as shown in Figure 7(a) and (b), respectively. The slightly higher exposure dose in one of the three exposures is evident in the different constituent structures in Figure 7(a).

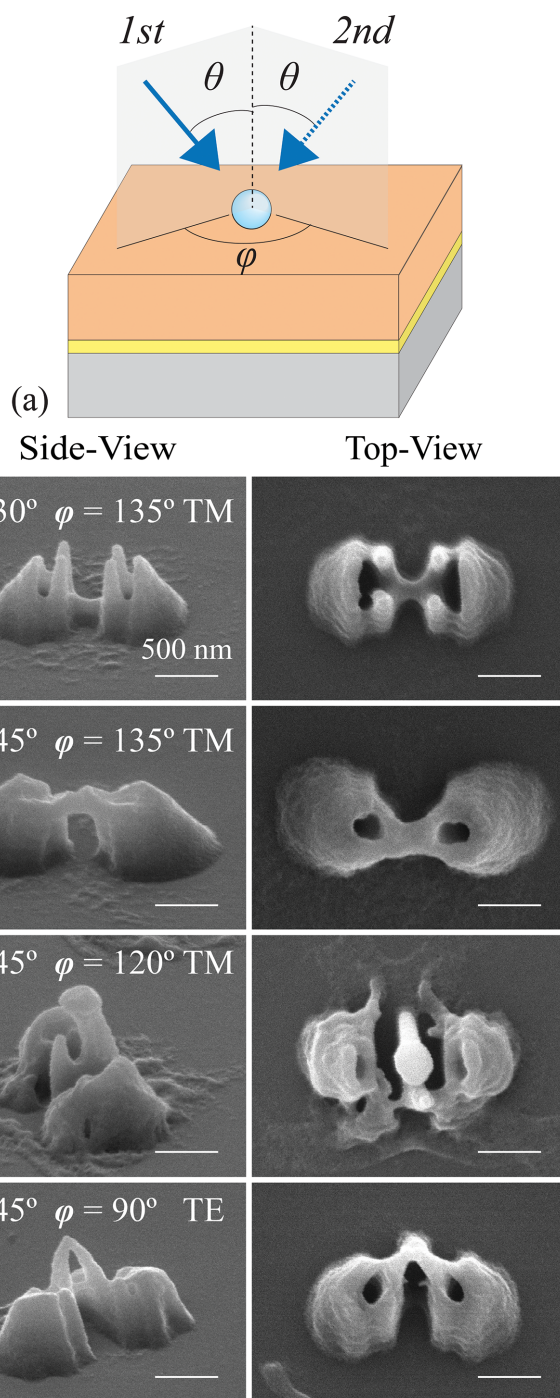


Figure 6. Micrographs of the nanostructures from sequential noncoplanar double exposures using 325 nm linearly polarized illumination. (a) Schematic of the exposure configuration. Side and top views of the nanostructures fabricated at (b) $\theta = 30^\circ$, $\phi = 135^\circ$, $D = 390 \text{ nm}$, exposure dose of 132 mJ cm^{-2} under TM exposures; (c) $\theta = 45^\circ$, $\phi = 135^\circ$, $D = 390 \text{ nm}$, exposure dose of 125 mJ cm^{-2} under TM exposures; (d) $\theta = 45^\circ$, $\phi = 120^\circ$, $D = 500 \text{ nm}$, exposure dose of 125 mJ cm^{-2} under TM exposures; (e) $\theta = 45^\circ$, $\phi = 90^\circ$, $D = 390 \text{ nm}$, exposure dose of 151 mJ cm^{-2} under TE exposures.

The results from quadruple exposures using TM polarization show four-fold symmetry, as shown in Figure 7(c)-(d). For a 390 nm diameter sphere, the four hollow structures by each exposure are connected to form a cross-like nanostructure

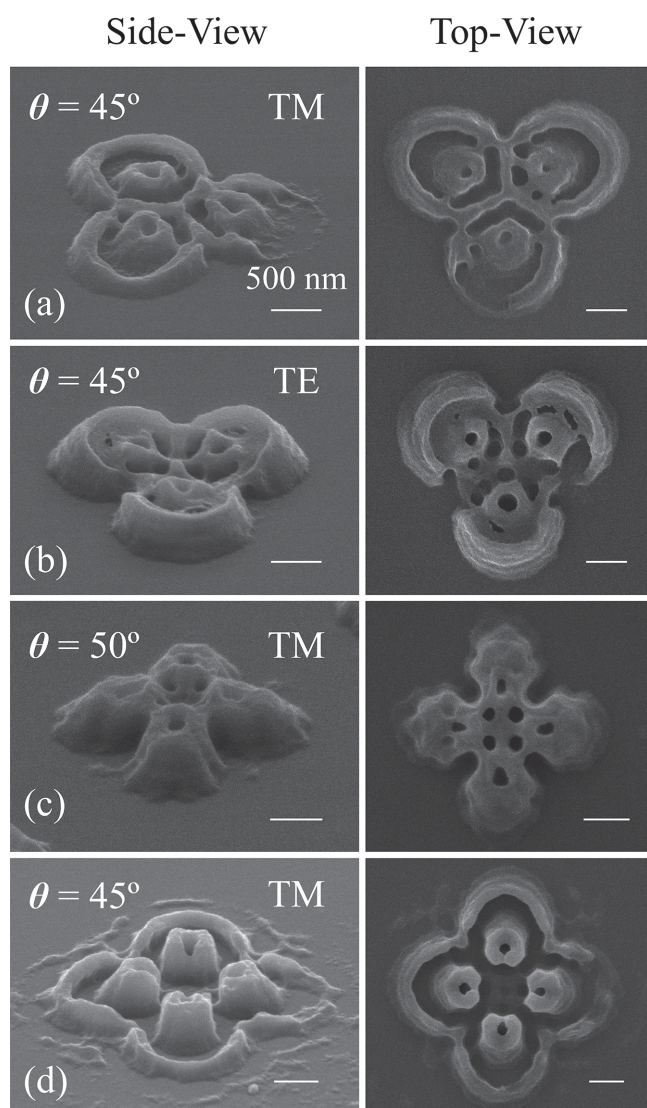


Figure 7. Micrographs of nanostructures fabricated under (a,b) triple and (c,d) quadruple symmetric exposures at incident angle θ . Side and top views of the nanostructures fabricated at (a) $\theta = 45^\circ$, $D = 500$ nm, exposure dose of 120 mJ cm^{-2} under TM exposures; (b) $\theta = 45^\circ$, $D = 500$ nm, exposure dose of 138 mJ cm^{-2} under TE exposures; (c) $\theta = 50^\circ$, $D = 390$ nm, exposure dose of 110 mJ cm^{-2} under TM exposures; (d) $\theta = 45^\circ$, $D = 500$ nm, exposure dose of 115 mJ cm^{-2} under TM exposures.

with four more holes in the central region, as shown in Figure 7(c). For a 500 nm diameter sphere, the four hollow structures are separate and surrounded by a second shell, as shown in Figure 7(d). Note that the different geometries in Figure 7(c) and (d) are mainly due to the different sphere sizes, resulting in the dramatic change of the scattered light distributions, which is characteristic of Mie scattering. These structures may find applications in resonant photonic structures. More complicated structures can potentially be enabled by additional illuminations. However, the number of exposures is limited by contrast degradation, which can lead to structure collapse. The reduction in exposure contrast also led to rougher surface morphology, which can be readily observed in structures fabricated using triple and quadruple exposures.

In our experiments, the exposures are applied sequentially so that the resultant structures are from the incoherent energy summations of the multiple scattering patterns. Interference effects using lasers can be exploited using simultaneous multiple-beam exposures that are mutually coherent. The coherent multiple illuminations are also expected to prevent contrast degradation, a limiting factor in incoherence multiple exposures. The multiple exposure configurations can also be further adjusted, such as varying sequential exposure doses, polarizations and incident angles of the individual exposures to further induce asymmetry. In this work the particle diameters were selected to be near the illumination wavelength of 325 nm to generate complex intensity patterns in the Mie scattering regime. Much larger and smaller particles can also be illuminated using light with corresponding wavelengths to obtain scaled versions of the demonstrated structures. Thus, there are many possible combinations of these configurable parameters, and the demonstrated structures are a limited subset of the proposed technique.

The fabrication of slanted nanostructure in a periodic array was investigated to examine its macroscopic material properties. In this process, close-packed polystyrene microsphere arrays were reduced into non-close-packed hexagonal lattice using isotropic oxygen plasma etching.^[62] Upon 325 nm TM-polarized illumination at incident angles of 30° and 60° , two slanted nanostructure arrays were fabricated, as shown in **Figure 8**. Only the first shell exists for both cases while the second shell collapses due to the interference effect between neighboring scattering patterns. It is important that the spacing between the particles must be sufficiently large so the scattering patterns from adjacent spheres do not overlap, which can result in structures with porous side walls. The structure spacing can also be increased by using larger spheres; however this requires longer etching which can result in non-spherical particles for illumination. The structure array was fabricated over an area of $\sim 15 \text{ mm}^2$, and structure collapse due to particle assembly defects can be observed. Wetting properties of the slanted 3D nanostructure arrays were tested by measuring static contact angles in different directions in Supplementary Information D. The slanted 3D nanostructure arrays also have potential applications in drug delivery and nanoscale inkjet printing.^[9–14,63–65]

3. Conclusion

In this work, we have demonstrated the fabrication of asymmetric 3D hollow nanostructures using multiple oblique light illuminations on individual colloidal elements. The proposed method is based on particle-light interactions in close proximity, and does not require complex setup such as precision optics, lasers, and other hardware. The oblique illumination approach introduces more parameters to harness the light scattering intensity patterns, which can be controlled by tuning the particle sizes, incident angles, polarizations, and exposure configurations. Sidewall and center hole angles can be designed with good agreements between experimental data and theoretical models. Multiple illuminations can also be employed to overlay the scattering profile, resulting in

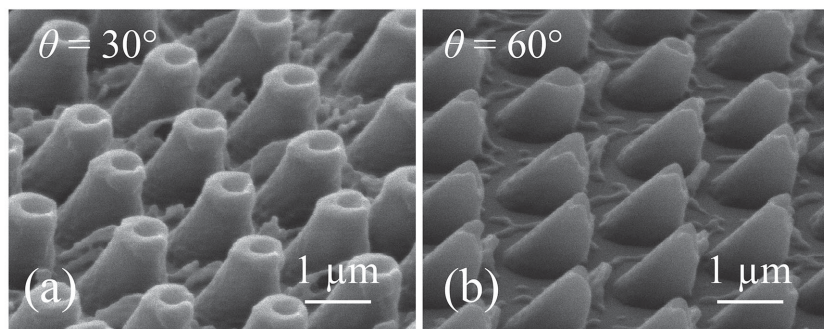


Figure 8. Micrographs of slanted nanostructure arrays fabricated using TM-polarized 325 nm illumination and 2 μm diameter original PS spheres. The structures were exposed at (a) $\theta = 30^\circ$ with dose of 135 mJ cm^{-2} and (b) $\theta = 60^\circ$ with dose of 190 mJ cm^{-2} .

more complex symmetries. Additional illumination configurations, such as exposure wavelength and coherence illumination can be included to further tailor the fabricated geometry. The slanted structures can also be fabricated in an ordered periodic array, which can find applications in nanoneedles for nanomaterial delivery, nanozzles for nanoink printing, and engineered surfaces with anisotropic wetting properties.

4. Experimental Section

Sample Preparation: In all experiments the samples were prepared on silicon substrates. A layer of antireflection coating (ARC i-CON-16, Brewer Science, Inc.) was used to reduce substrate back reflection. The antireflection coating thickness is 95 nm to minimize reflection from 325 nm wavelength normal incidence light. Positive photoresist (Sumitomo PFI88A7) was spincoated on the ARC layer. The thickness of the photoresist layer should be thick enough to capture the scattering pattern and depends on the choice of particle size. However, the thickness is limited by the photoresist material absorption, as light intensity decays exponentially into the material. For all experiments, 1 μm thickness was used. Monodispersed polystyrene spheres with diameters of 390 nm and 500 nm (Polyscience Polybead Microspheres in 2.5% aqueous solution) were used as scattering objects in the experiments. The solution was spincoated on the photoresist sample to assemble into isolated spheres. Before spincoating, the photoresist sample is dipped into the developer solution (Microposit MF-CD-26) for a few seconds and then immersed in DI water. After treatment, the photoresist surface becomes hydrophilic to sustain a water film to facilitate the spreading of nanospheres during assembly. The particle solution is diluted to 0.1% and spincoated at 1000 rpm to obtain isolated particle assemblies.

Lithographic exposures were performed using a linearly polarized 325 nm HeCd laser. After exposing the samples with doses of 100–450 mJ cm^{-2} , the nanospheres were removed by ultrasonic agitation. The exposed samples were then developed in tetramethylammonium hydroxide (TMAH, 2.4%) developer solution (Microposit MF-CD-26) for 1–2 min. The samples were characterized using top-view and cross-section-view scanning electron microscope (JEOL 6400F) at 5 KeV. The cross sections of individual nanostructures were obtained by cleaving the samples using a diamond scribe. The (100) silicon substrates used prefer to cleave along

crystalline planes, creating a clean cross section for SEM characterization. The structures shown broke along the center line by chance, which routinely occurs since there are many nanostructures within a sample. The wetting properties of the fabricated structures were characterized using a contact angle goniometer (Ramé-Hart Instrument Co., Model 200-F1).

Simulation and Modeling: The colloidal-light scattering intensity distribution in the photoresist was modeled using finite-difference time-domain (FDTD) methods. A binary photoresist model was used to predict the resulting structures, where any volume above a threshold dose was completely removed.

The geometries of the simulated structures are then quantitatively analyzed in Matlab. The predicted models are depicted as inset diagrams with their corresponding fabrication results. For more details on simulation setup and binary resist model, see Supplementary Information A.

Supporting Information

Supporting Information is available from the Wiley Online Library or from the author.

Acknowledgements

We gratefully acknowledge the students, staff, and facility support from the North Carolina State University Nanofabrication Facility (NNF) and Analytical Instrumentation Facility (AIF). This work was supported by a NASA Office of the Chief Technologist's Space Technology Research Opportunity – Early Career Faculty grant (grant NNX12AQ46G) and by the National Science Foundation (grant EEC-1160483) through the Nanosystems Engineering Research Center for Advanced Self-Powered Systems of Integrated Sensors and Technologies (ASSIST).

- [1] S. Y. Lin, J. G. Fleming, D. L. Hetherington, B. K. Smith, R. Biswas, K. M. Ho, M. M. Sigalas, W. Zubrzycki, S. R. Kurtz, J. Bur, *Nature* **1998**, 394, 251.
- [2] S. Noda, K. Tomoda, N. Yamamoto, A. Chutinan, *Science* **2000**, 289, 604.
- [3] M. Qi, E. Lidorikis, P. T. Rakich, S. G. Johnson, J. D. Joannopoulos, E. P. Ippen, H. I. Smith, *Nature* **2004**, 429, 538.
- [4] J.-H. Jang, C. K. Ullal, T. Gorishnyy, V. V. Tsukruk, E. L. Thomas, *Nano Lett.* **2006**, 6, 740.
- [5] Z. Fan, H. Razavi, J. Do, A. Moriwaki, O. Ergen, Y.-L. Chueh, P. W. Leu, J. C. Ho, T. Takahashi, L. A. Reichertz, S. Neale, K. Yu, M. Wu, J. W. Ager, A. Javey, *Nat. Mater.* **2009**, 8, 648.
- [6] H. Zhang, X. Yu, P. V. Braun, *Nat. Nanotechnol.* **2011**, 6, 277.
- [7] W.-L. Min, B. Jiang, P. Jiang, *Adv. Mater.* **2008**, 20, 3914.
- [8] K.-C. Park, H. J. Choi, C.-H. Chang, R. E. Cohen, G. H. McKinley, G. Barbastathis, *ACS Nano* **2012**, 6, 3789.

- [9] X. W. (David) Lou, L. A. Archer, Z. Yang, *Adv. Mater.* **2008**, *20*, 3987.
- [10] M. S. Yavuz, Y. Cheng, J. Chen, C. M. Cobley, Q. Zhang, M. Rycenga, J. Xie, C. Kim, K. H. Song, A. G. Schwartz, L. V. Wang, Y. Xia, *Nat. Mater.* **2009**, *8*, 935.
- [11] G. D. Moon, S.-W. Choi, X. Cai, W. Li, E. C. Cho, U. Jeong, L. V. Wang, Y. Xia, *J. Am. Chem. Soc.* **2011**, *133*, 4762.
- [12] E. Peer, A. Artyz-Schnirman, L. Gepstein, U. Sivan, *ACS Nano* **2012**, *6*, 4940.
- [13] M. R. Prausnitz, S. Mitragotri, R. Langer, *Nat. Rev. Drug Discov.* **2004**, *3*, 115.
- [14] M. R. Prausnitz, R. Langer, *Nat. Biotechnol.* **2008**, *26*, 1261.
- [15] Y. Yao, J. Yao, V. K. Narasimhan, Z. Ruan, C. Xie, S. Fan, Y. Cui, *Nat. Commun.* **2012**, *3*, 664.
- [16] F. De Angelis, M. Malerba, M. Patrini, E. Miele, G. Das, A. Toma, R. P. Zaccaria, E. Di Fabrizio, *Nano Lett.* **2013**, *13*, 3553.
- [17] B. Ai, Y. Yu, H. Möhwald, G. Zhang, *Adv. Optical Mater.* **2013**, *1*, 724.
- [18] S. Tawfick, M. De Volder, D. Copic, S. J. Park, C. R. Oliver, E. S. Polsen, M. J. Roberts, A. J. Hart, *Adv. Mater.* **2012**, *24*, 1628.
- [19] W. R. Hansen, K. Autumn, *Proc. Natl. Acad. Sci. USA* **2005**, *102*, 385.
- [20] Y. Zheng, X. Gao, L. Jiang, *Soft Matter* **2007**, *3*, 178.
- [21] H. E. Jeong, J.-K. Lee, H. N. Kim, S. H. Moon, K. Y. Suh, *Proc. Natl. Acad. Sci. USA* **2009**, *106*, 5639.
- [22] D. Sameoto, C. Menon, *Smart Mater. Structures* **2010**, *19*, 103001.
- [23] L. Ge, S. Sethi, L. Ci, P. M. Ajayan, A. Dhinojwala, *Proc. Natl. Acad. Sci. USA* **2007**, *104*, 10792.
- [24] T. Kim, H. E. Jeong, K. Y. Suh, H. H. Lee, *Adv. Mater.* **2009**, *21*, 2276.
- [25] Y. Rahmawan, T. Kim, S. J. Kim, K.-R. Lee, M.-W. Moon, K.-Y. Suh, *Soft Matter* **2012**, *8*, 1673.
- [26] N. A. Malvadkar, M. J. Hancock, K. Sekeroglu, W. J. Dressick, M. C. Demirel, *Nat. Mater.* **2010**, *9*, 1023.
- [27] K.-H. Chu, R. Xiao, E. N. Wang, *Nat. Mater.* **2010**, *9*, 413.
- [28] H. C. Jeon, T. Y. Jeon, S.-M. Yang, *ACS Appl. Mater. Interfaces* **2013**, *5*, 9791.
- [29] M. F. L. D. Volder, S. J. Park, S. H. Tawfick, D. O. Vidaud, A. J. Hart, *J. Micromech. Microeng.* **2011**, *21*, 045033.
- [30] M. De Volder, A. J. Hart, *Angew. Chem. Int. Ed.* **2013**, *52*, 2412.
- [31] M. Han, W. Lee, S.-K. Lee, S. S. Lee, *Sens. Actuat. A* **2004**, *111*, 14.
- [32] H. Sato, D. Yagyu, S. Ito, S. Shoji, *Sens. Actuat. A* **2006**, *128*, 183.
- [33] G. Jiang, S. Baig, M. R. Wang, *J. Micromech. Microeng.* **2012**, *22*, 085022.
- [34] S. M. Lubin, W. Zhou, A. J. Hryn, M. D. Huntington, T. W. Odom, *Nano Lett.* **2012**, *12*, 4948.
- [35] A. van Blaaderen, R. Ruel, P. Wiltzius, *Nature* **1997**, *385*, 321.
- [36] B. Gates, D. Qin, Y. Xia, *Adv. Mater.* **1999**, *11*, 466.
- [37] M. Rycenga, P. H. C. Camargo, Y. Xia, *Soft Matter* **2009**, *5*, 1129.
- [38] Y. Xia, B. Gates, Y. Yin, Y. Lu, *Adv. Mater.* **2000**, *12*, 693.
- [39] J. C. Love, B. D. Gates, D. B. Wolfe, K. E. Paul, G. M. Whitesides, *Nano Lett.* **2002**, *2*, 891.
- [40] J. C. Hulteen, R. P. V. Duyne, *J. Vacuum Sci. Technol. A* **1995**, *13*, 1553.
- [41] C. Haginoya, M. Ishibashi, *Appl. Phys. Lett.* **1997**, *71*, 2934.
- [42] J. H. Moon, W. S. Kim, J.-W. Ha, S. G. Jang, S.-M. Yang, J.-K. Park, *Chem. Commun.* **2005**, 4107.
- [43] T. Wang, J. Zhang, X. Zhang, P. Xue, H. Chen, X. Li, Y. Yu, B. Yang, *J. Mater. Chem. C* **2013**, *1*, 1122.
- [44] M. Fang, H. Lin, H.-Y. Cheung, S. Yip, F. Xiu, C.-Y. Wong, J. C. Ho, *Adv. Optical Mater.* **2014**, DOI: 10.1002/adom.201400127.
- [45] T. Y. Jeon, H. C. Jeon, S. Y. Lee, T. S. Shim, J.-D. Kwon, S.-G. Park, S.-M. Yang, *Adv. Mater.* **2014**, *26*, 1422.
- [46] S.-M. Yang, S. G. Jang, D.-G. Choi, S. Kim, H. K. Yu, *Small* **2006**, *2*, 458.
- [47] P. Kühler, F. J. García de Abajo, J. Solis, M. Mosbacher, P. Leiderer, C. n. Afonso, J. Siegel, *Small* **2009**, *5*, 1825.
- [48] C. David, P. Kühler, F. Javier García de Abajo, J. Siegel, *Opt. Express* **2014**, *22*, 8226.
- [49] W. Wu, A. Katsnelson, O. G. Memis, H. Mohseni, *Nanotechnology* **2007**, *18*, 485302.
- [50] E. Mcleod, C. B. Arnold, *Nat. Nano* **2008**, *3*, 413.
- [51] Y. Zhang, T. Wei, Z. Xiong, L. Shang, Y. Tian, Y. Zhao, P. Zhou, J. Wang, J. Li, *Appl. Phys. Lett.* **2014**, *105*, 013108.
- [52] C.-H. Chang, L. Tian, W. R. Hesse, H. Gao, H. J. Choi, J.-G. Kim, M. Siddiqui, G. Barbastathis, *Nano Lett.* **2011**, *11*, 2533.
- [53] X. A. Zhang, J. Elek, C.-H. Chang, *ACS Nano* **2013**, *7*, 6212.
- [54] K. Yamazaki, H. Yamaguchi, *J. Vac. Sci. Technol., B* **2008**, *26*, 2529.
- [55] J.-H. Jang, C. K. Ullal, M. Maldovan, T. Gorishnyy, S. Kooi, C. Koh, E. L. Thomas, *Adv. Funct. Mater.* **2007**, *17*, 3027.
- [56] S. Kawata, H.-B. Sun, T. Tanaka, K. Takada, *Nature* **2001**, *412*, 697.
- [57] W. Haske, V. W. Chen, J. M. Hales, W. Dong, S. Barlow, S. R. Marder, J. W. Perry, *Opt. Express* **2007**, *15*, 3426.
- [58] J. K. Gansel, M. Thiel, M. S. Rill, M. Decker, K. Bade, V. Saile, G. von Freymann, S. Linden, M. Wegener, *Science* **2009**, *325*, 1513.
- [59] Y. Xia, Y. Xiong, B. Lim, S. E. Skrabalak, *Angew. Chem. Int. Ed.* **2009**, *48*, 60.
- [60] J. Henzie, M. Grünwald, A. Widmer-Cooper, P. L. Geissler, P. Yang, *Nat. Mater.* **2012**, *11*, 131.
- [61] A. F. Oskooi, D. Roundy, M. Ibanescu, P. Bermel, J. D. Joannopoulos, S. G. Johnson, *Computer Phys. Commun.* **2010**, *181*, 687.
- [62] A. Plettl, F. Enderle, M. Saitner, A. Manzke, C. Pfahler, S. Wiedemann, P. Ziemann, *Adv. Funct. Mater.* **2009**, *19*, 3279.
- [63] J.-U. Park, M. Hardy, S. J. Kang, K. Barton, K. Adair, D. Kishore Mukhopadhyay, C. Y. Lee, M. S. Strano, A. G. Alleyne, J. G. Georgiadis, P. M. Ferreira, J. A. Rogers, *Nat. Mater.* **2007**, *6*, 782.
- [64] Z. Dong, J. Ma, L. Jiang, *ACS Nano* **2013**, *7*, 10371.
- [65] O. Loh, R. Lam, M. Chen, N. Moldovan, H. Huang, D. Ho, H. D. Espinosa, *Small* **2009**, *5*, 1667.

Received: September 11, 2014

Revised: October 9, 2014

Published online: